Classification of time-reversal symmetric topological superconducting phases for conventional pairing symmetries

Seishiro Ono,[1,*] Ken Shiozaki,[2,†] and Haruki Watanabe[1,‡]
[1]*Department of Applied Physics, University of Tokyo, Tokyo 113-8656, Japan*
[2]*Center for Gravitational Physics and Quantum Information, Yukawa Institute for Theoretical Physics, Kyoto University, Kyoto 606-8502, Japan*

(Received 4 April 2023; revised 10 December 2023; accepted 11 April 2024; published 3 June 2024)

Symmetry properties of Cooper pairs play a pivotal role in studies on topological superconductivity. Unconventional superconductors, whose pairing symmetries are different from conventional Bardeen-Cooper-Schrieffer superconductors, have been paid attention to as a platform of topological superconductivity. However, pairing symmetries of most superconductors are actually the conventional one and these superconductors are usually considered to be topologically trivial. In this work, combining the real-space and the momentum space approaches developed recently, we conduct classifications of time-reversal symmetric topological superconductors with conventional pairing symmetries. Remarkably, we find topological superconducting phases in 199 out of 230 space groups. Our finding sheds light on superconductors with conventional pairing symmetries as candidates for topological superconductors.

DOI: 10.1103/PhysRevB.109.214502

I. INTRODUCTION

In past decades, topological superconductors (TSCs) have attracted much attention because of their exotic surface states that realize Majorana fermions. Majorana fermions could be leveraged for fault-tolerant quantum computation [1]. Topological superconducting phases protected by internal symmetries, particle-hole symmetry (PHS), and time-reversal symmetries (TRS) are discovered in the early stages of studies of TSCs [2–4]. Symmetry properties of Cooper pairs, often called pairing symmetries, are closely related to the topological nature of superconductivity.

Crystalline symmetry plays a pivotal role in superconductors. Pairing symmetries are classified into irreducible representations of point groups [5]. Recent intensive studies reveal that unconventional superconductors, whose pairing symmetries are distinct from conventional Bardeen-Cooper-Schrieffer (BCS) superconductivity, have a great chance of being TSCs [6–16]. For instance, odd-parity superconductors are promising candidates for TSCs [17,18]. Furthermore, thanks to the bloom in understanding of TSCs protected by crystalline symmetries [19–45], it is known that topological superconducting phases can also exist for even-parity but unconventional pairing symmetries [32,34,36,46,47]. Unfortunately, however, unconventional superconductivity is quite rare and most superconductors exhibit conventional pairing symmetries.

Then, it is crucial to understand the topological nature of superconductors whose order parameters transform in the same way as the BCS superconductor does under point group symmetry. Such a superconducting order parameter is said to have a conventional pairing symmetry. Several studies actually show the existence of topological phases for conventional pairing symmetries. For example, for noncentrosymmetric superconductors in which even-parity and odd-parity components are allowed to be mixed, TSCs protected by TRS and PHS can be realized when the odd-parity component is comparable to or larger than the even-parity one [48]. More recently, Ref. [49] has reported a topological superconducting phase for conventional pairing symmetry in centrosymmetric space group $P4/nmm$ (No. 129). It should be noted that sign-changing pair potentials, dubbed extended s- or $s_{\pm}$-wave pairings, are required to realize this phase [49–51]. However, despite intense research efforts, the list of topological phases for conventional pairing symmetries is still elusive in most space groups.

In principle, TSCs could be classified by K-theory [23,52–54], but the actual calculation is often challenging. Recently, an alternative approach has been introduced based on a real-space perspective [55–64], which is called Atiyah-Hirzebruch spectral sequence (AHSS) [59] in real space or topological crystals [60,65]. The idea of this method is that any topological crystalline phase can be constructed by symmetrically placing lower-dimensional topological phases. It has actually succeeded in comprehensively classifying topological insulators [60,65] and bosonic systems [56,58,63,64]. It should be stressed that the components of lower-dimensional topological phases are completely decoupled. Although realistic systems are usually much more complicated, they are believed to be deformable to such decoupling limits without closing the gap. In this sense, the real-space approach works for classification problems.

*seishiro.ono@riken.jp; Present address: Interdisciplinary Theoretical and Mathematical Sciences Program (iTHEMS), RIKEN, Wako 351-0198, Japan.
†ken.shiozaki@yukawa.kyoto-u.ac.jp
‡hwatanabe@g.ecc.u-tokyo.ac.jp

In this work, we generalize the method to superconductors. There are two complications in the real-space classification for superconductors, compared with the case for insulators. For one, we find one-dimensional building block TSCs that bring out some technical differences in the classification procedures. In addition, we discover an obstruction to constructing gapped phases. The existence of superconducting vortices with odd-integer windings can be enforced by crystalline symmetries. Consequentially, Majorana zero modes emerge at the vortex cores.

We overcome these difficulties and provide real-space classifications of time-reversal symmetric TSCs with conventional pairing symmetries in all rod groups, layer groups, and space groups. Importantly, we find that there exist topological superconducting phases in 199 out of 230 space groups (61 centrosymmetric and 138 noncentrosymmetric space groups). Since pairing symmetries of most realistic materials are conventional as mentioned above, our study will stimulate further studies of topological superconductivity in realistic materials that have already been verified or will be discovered in the future.

II. OVERVIEW OF REAL-SPACE CLASSIFICATION

Our classification of topological superconductors in this work is based on the framework developed in previous studies [55,56,58,59,61]. Consider a symmetry group $G = \mathcal{G}_{\rm int} \times \mathcal{G}$, where $\mathcal{G}_{\rm int}$ and $\mathcal{G}$ are an internal symmetry group and a space group. The classification of topological crystalline phase with symmetry G is based on a conjecture: any topological crystalline phase can be adiabatically deformed into a $\mathcal{G}$-symmetric patchwork of lower-dimensional invertible topological phases protected by internal symmetries of the subspace [55,56]. Under this assumption, the classification of gapped topological crystalline phases is equivalent to the classification of patchworks that do not contain any gapless mode in the bulk.

Before moving on to the concrete classification procedures, let us define pairing symmetries formally. Let $\hat{c}^\dagger_{\boldsymbol{k},\sigma}$ be a fermionic creation operator with momentum $\boldsymbol{k}$ and a degree of freedom $\sigma \in \{1, 2, \ldots, N_{\rm orb}\}$. A symmetry $g \in \mathcal{G}$ transforms $\hat{c}^\dagger_{\boldsymbol{k},\sigma}$ into another creation operator, as implemented by

$$\hat{g}\hat{c}^\dagger_{\boldsymbol{k},\sigma}\hat{g}^{-1} = \hat{c}^\dagger_{g\boldsymbol{k},\sigma'}[u_{\boldsymbol{k}}(g)]_{\sigma'\sigma}, \tag{1}$$

where $u_{\boldsymbol{k}}(g)$ is a unitary matrix. When the symmetry g is present in the superconducting phase, the order parameter $\hat{\Delta} = \frac{1}{2}\sum_{\boldsymbol{k}}\sum_{\sigma,\sigma'}[\Delta_{\boldsymbol{k}}]_{\sigma\sigma'}\hat{c}^\dagger_{\boldsymbol{k},\sigma}\hat{c}^\dagger_{-\boldsymbol{k},\sigma'} + \text{H.c.}$ is also symmetric under g, i.e., $\hat{g}\hat{\Delta}\hat{g}^{-1} = \hat{\Delta}$. To satisfy this, $\Delta_{\boldsymbol{k}}$ is also transformed as

$$u_{\boldsymbol{k}}(g)\Delta_{\boldsymbol{k}}u^T_{-\boldsymbol{k}}(g) = e^{i\theta_g}\Delta_{g\boldsymbol{k}}, \tag{2}$$

where $\theta_g \in \mathbb{R}$ [66]. In the presence of TRS, $\theta_g = 0$ or $\pi \bmod 2\pi$. A pairing symmetry is given by $\{e^{i\theta_g}\}_{g\in\mathcal{G}}$. We say that the pairing symmetry is conventional if $e^{i\theta_g} = +1$ for $^\forall g \in \mathcal{G}$. When there exists $g \in \mathcal{G}$ such that $e^{i\theta_g} \neq +1$, we say the pairing symmetry is unconventional. It should be emphasized that the term "conventional pairing symmetry" does not always mean the conventional BCS-type pairing. For example, consider a quasi-one-dimensional spinless superconducting system with a single-band normal conducting phase. We further assume that the system is symmetric under reflection M_y about y direction. Then, it is possible to realize p-wave pairings, say $\Delta_{k_x} = \sin k_x$, that satisfy $u_{k_x}(M_y)\Delta_{k_x}u^T_{-k_x}(M_y) = +\Delta_{k_x}$. Another example is an extended s-wave or $s_\pm$-wave pairing, which is not a BCS-type pairing but has conventional pairing symmetry.

For superconductors with conventional pairing symmetries, the classification can be performed in the following steps (A)–(E).

(A) Decomposing unit cell: three-dimensional (3D) space is decomposed into p-dimensional regions for $p = 0,\ 1,\ 2,$ and 3, which are called p-cells. Each p-cell should be chosen small enough so that any two points in a p-cell are not symmetry related to each other. To define 3-cells, we choose a closed and simply connected region that covers the entire space by symmetry operations exactly once. Such a region is known as an asymmetric unit (AU) [67] and can be chosen as a polyhedron. The AU is divided into M subregions ($M \geqslant 1$). The interiors of these subregions and their symmetric copies are 3-cells. In general, M can be set to 1, but sometimes other choices are convenient. The 2-cells are polygons on faces of 3-cells. Similarly, 1-cells are line segments along the edges of 2-cells. End points of 1-cells are 0-cells. This decomposition is referred to as *cell decomposition*. Although the cell decomposition for a given symmetry setting is not unique, the classification outcome does not depend on the choice.

(B) Identifying building blocks: for each p-cell, we determine its symmetry group, which is composed of $\mathcal{G}_{\rm int}$ and the subgroup of $\mathcal{G}$ that behaves as an internal symmetry group on the p-cell. For time-reversal symmetric superconductors with significant spin-orbit coupling (SOC), $\mathcal{G}_{\rm int}$ is generated by the time-reversal symmetry with $\mathcal{T}^2 = -1$ and the particle-hole symmetry $\mathcal{C}^2 = +1$. On each p-cell, we list all p-dimensional TSCs protected by the symmetry group of the p-cell. According to Refs. [3,4], for conventional pairing symmetries, there are four building blocks: 3D $\mathbb{Z}$-TSC on 3-cells, 2D $\mathbb{Z}_2$-TSC on 2-cells whose symmetry is $\mathcal{G}_{\rm int}$ only (i.e., without an additional mirror), and 1D $\mathbb{Z}_2$-TSC or 1D $\mathbb{Z}$-TSC on 1-cells depending on the symmetry of the cell.

(C) Constructing boundary-gapped patchwork: we construct patchworks by symmetrically arranging these building blocks. A TSC on a p-cell exhibits $(p-1)$-dimensional gapless boundary modes. We demand that boundary modes in a patchwork be gapped among them. We refer to patchworks obtained this way as *boundary-gapped patchworks*. We identify boundary-gapped patchworks that can be deformed into each other.

(D) Checking the absence of vortex zero modes: we check if a boundary-gapped patchwork is *fully gapped*. Patchworks constructed by 2D TSCs may still contain vortex zero modes, as seen in Sec. III. Since the spectrum is gapless in the presence of vortex zero modes, we require the absence of such zero modes to classify gapped TSCs. To achieve this, we eliminate vortex zero modes from patchworks by considering combinations of boundary-gapped patchworks, as discussed in Sec. III. This step is unique to superconductors and was not necessary in previous studies for insulators and bosonic systems [58,60,65]. A fully gapped patchwork constructed from nontrivial TSCs on p-cell gives an element of an Abelian

group $E^{\infty}_{p,-p} = (\mathbb{Z}_2)^{n_p} \times \mathbb{Z}^{m_p}$ with non-negative integers n_p and m_p (see the Supplemental Material). Let us comment on the physical consequences of $\{E^{\infty}_{p,-p}\}_{p=1,2,3}$. As seen from the above discussions, nontrivial elements of $E^{\infty}_{1,-1}$ and $E^{\infty}_{2,-2}$ are constructed from 1D TSCs and 2D TSCs, respectively. These TSCs can be understood as so-called weak or higher-order TSCs. On the other hand, nontrivial elements of $E^{\infty}_{3,-3}$ represent the so-called strong TSCs protected by the 3D winding numbers. As a result, there is a simple criterion for $E^{\infty}_{3,-3}$. Let $p_g \in \mathrm{O}(3)$ be a matrix that represents a real-space transformation of the point-group part of g. If $\det p_g = +1$ for $^{\forall}g \in \mathcal{G}$, the 3D winding number can be nontrivial, i.e., $E^{\infty}_{3,-3} = \mathbb{Z}$. Otherwise, the 3D winding number must be zero, namely, $E^{\infty}_{3,-3} = 0$.

(E) Determining K-theoretic classifications: as the last step we want to determine the Abelian group of these topological phases, which is given by K-group. The Abelian group $E^{\infty}_{p,-p}$ was computed separately for each $p = 1, 2, 3$ and, in general, $\oplus^{3}_{p=1} E^{\infty}_{p,-p}$ does not reproduce the K-group result, because $E^{\infty}_{p,-p}$ $(p = 1, 2, 3)$ are not mutually independent. For example, a patchwork obtained by stacking several copies of nontrivial patchworks in $E^{\infty}_{2,-2}$ is sometimes equivalent to a nontrivial patchwork in $E^{\infty}_{1,-1}$. To identify the group structure among $E^{\infty}_{p,-p}$, we have to solve the group extension problem [59,68], as we will discuss later.

Space group $P\bar{1}$: let us illustrate the above steps [other than step (E)] through discussing space group $P\bar{1}$, generated by translations and inversion, as an example. The AU is chosen as the gray region in Fig. 1(a) with $0 \leqslant x \leqslant 1/2$, $0 \leqslant y < 1$, and $0 \leqslant z < 1$. A cell decomposition is shown in Fig. 1(b). The interior of AU gives a 3-cell. Its face on $x = 1/2$ (i.e., $0 \leqslant y < 1$ and $0 \leqslant z < 1$) contains inversion centers [red points in Fig. 1(b)] and every point on the face is mapped to another point on the same face by inversion. Hence the face should be divided into two 2-cells, one of which is shown by a green triangle in Fig. 1(b). Similarly, edges of 2-cells that contain inversion centers must be decomposed into two 1-cells, one of which is shown by a thick line in Fig. 1(b). This is the end of step (A). Step (B) is common among almost all space groups. Since the symmetry of all 1- and 2-cells is $\mathcal{G}_{\mathrm{int}}$ only, these cells host 1D $\mathbb{Z}_2$-TSCs and 2D $\mathbb{Z}_2$-TSCs.

Now we move on to step (C). We first consider 1D $\mathbb{Z}_2$-TSCs on 1-cells. There are seven symmetry-inequivalent 1-cells, generating in 2^7 patterns of patchworks. Note that end points of 1-cells are inversion centers. Hence every TSC on a 1-cell meets with its inversion copy at end points. However, the two Majorana-Kramers zero modes sitting at the inversion center cannot be gapped, because they have different inversion eigenvalues. This point can be understood by noting that the inversion is represented by τ_x (Pauli matrix) whose eigenvalues are ± 1 [see Fig. 1(c)]. Therefore, in the current cell decomposition, there are no boundary-gapped patchworks composed of 1D TSCs. One might choose a different cell decomposition and put 1D $\mathbb{Z}_2$-TSCs in such a way that four Majorana-Kramers zero modes meet at each inversion center to make a boundary-gapped patchwork as illustrated in Fig. 1(d). However, such a configuration can be deformed into the vacuum. We conclude that $E^{\infty}_{1,-1} = 0$ regardless of the choice of the cell decomposition.

We next consider patchworks composed of 2D $\mathbb{Z}_2$-TSCs. There are four symmetry-inequivalent 2-cells. We consider configurations obtained by placing a 2D TSC on one of them [see in Fig. 1(e)]. Since two helical edge modes always meet on each of the boundary 1-cells, they can be gapped in pairs. Thus all of these configurations are boundary-gapped patchworks.

Step (D) is the novel part of the classification. As we elaborate below, these boundary-gapped patchworks constructed from 2D $\mathbb{Z}_2$-TSCs are not fully gapped because vortex zero modes survive at inversion centers. To get rid of vortex zero modes, an even number of 2D $\mathbb{Z}_2$-TSCs must be crossing at each inversion center. However, such a combination of four planes in Fig. 1(e) does not exist in this cell decomposition. When a different cell decomposition is assumed, such a configuration may be realized, but then it can be smoothly deformed into the vacuum as shown in Fig. 1(f). Thus we conclude $E^{\infty}_{2,-2} = 0$ regardless of the choice of the cell decomposition.

III. CONSTRUCTION OF FULLY GAPPED PATCHWORKS

As discussed in the preceding section, boundary gapped patchworks constructed by 2D TSCs are sometimes gapless due to the presence of vortex zero modes. In this section, we discuss how to obtain fully gapped patchworks.

A. Superconducting vortices

In the presence of a vortex (with the unit winding) in the superconducting order parameter, 2D $p_x \pm ip_y$ superconductors have a Majorana zero mode at the core of the vortex [69–73]. The zero mode can be described by a continuum model

$$H_{\pm}(\boldsymbol{r};\Delta) = \begin{pmatrix} -\frac{\nabla^2}{2m} - \mu(\boldsymbol{r}) & \Delta(\boldsymbol{r})\left(\frac{1}{i}\partial_x \pm i\frac{1}{i}\partial_y\right) \\ \Delta^*(\boldsymbol{r})\left(\frac{1}{i}\partial_x \mp i\frac{1}{i}\partial_y\right) & \frac{\nabla^2}{2m} + \mu(\boldsymbol{r}) \end{pmatrix}, \tag{3}$$

where PHS is represented by τ_x. The superconducting gap function $\Delta(\boldsymbol{r})$ and the chemical potential $\mu(\boldsymbol{r})$ vary slowly in space. To implement TRS with $\mathcal{T}^2 = -1$, we introduce a spin degree of freedom and use $H_+(\boldsymbol{r};\Delta)$ for the spin-up component and $H_-(\boldsymbol{r};\Delta^*)$ for the spin-down component. The resulting Hamiltonian reads

$$H_{\mathrm{DIII}}(\boldsymbol{r};\Delta) = H_+(\boldsymbol{r};\Delta) \otimes \begin{pmatrix} 1 & 0 \\ 0 & 0 \end{pmatrix} + H_-(\boldsymbol{r};\Delta^*) \otimes \begin{pmatrix} 0 & 0 \\ 0 & 1 \end{pmatrix}. \tag{4}$$

PHS and TRS are represented by $\tau_x s_0$ and $i\tau_z s_y$, respectively. In these expressions, the second matrix refers to the spin space and s_0 and s_i's are another set of Pauli matrices.

Here we argue that a 2D inversion symmetric TSC always has a vortex with an odd-integer winding at the inversion center and consequently has a Kramers pair of Majorana zero modes at the core of a vortex. Inversion symmetry is represented by τ_0 in $H_{\pm}(\boldsymbol{r};\Delta)$ and by $\tau_0 s_0$ in $H_{\mathrm{DIII}}(\boldsymbol{r};\Delta)$. We assume the form $\Delta(\boldsymbol{r}) = \Delta_0(r)e^{i(\alpha+n\theta)}$ and $\mu(\boldsymbol{r}) = \mu(r)$, where r and θ are polar coordinates and $\alpha \in \mathbb{R}$. From the symmetry condition $\tau_0 H_{\pm}(\boldsymbol{r};\Delta) = H_{\pm}(-\boldsymbol{r};\Delta)\tau_0$, we find $\Delta(-\boldsymbol{r}) = -\Delta(\boldsymbol{r})$, which implies that n is an odd integer

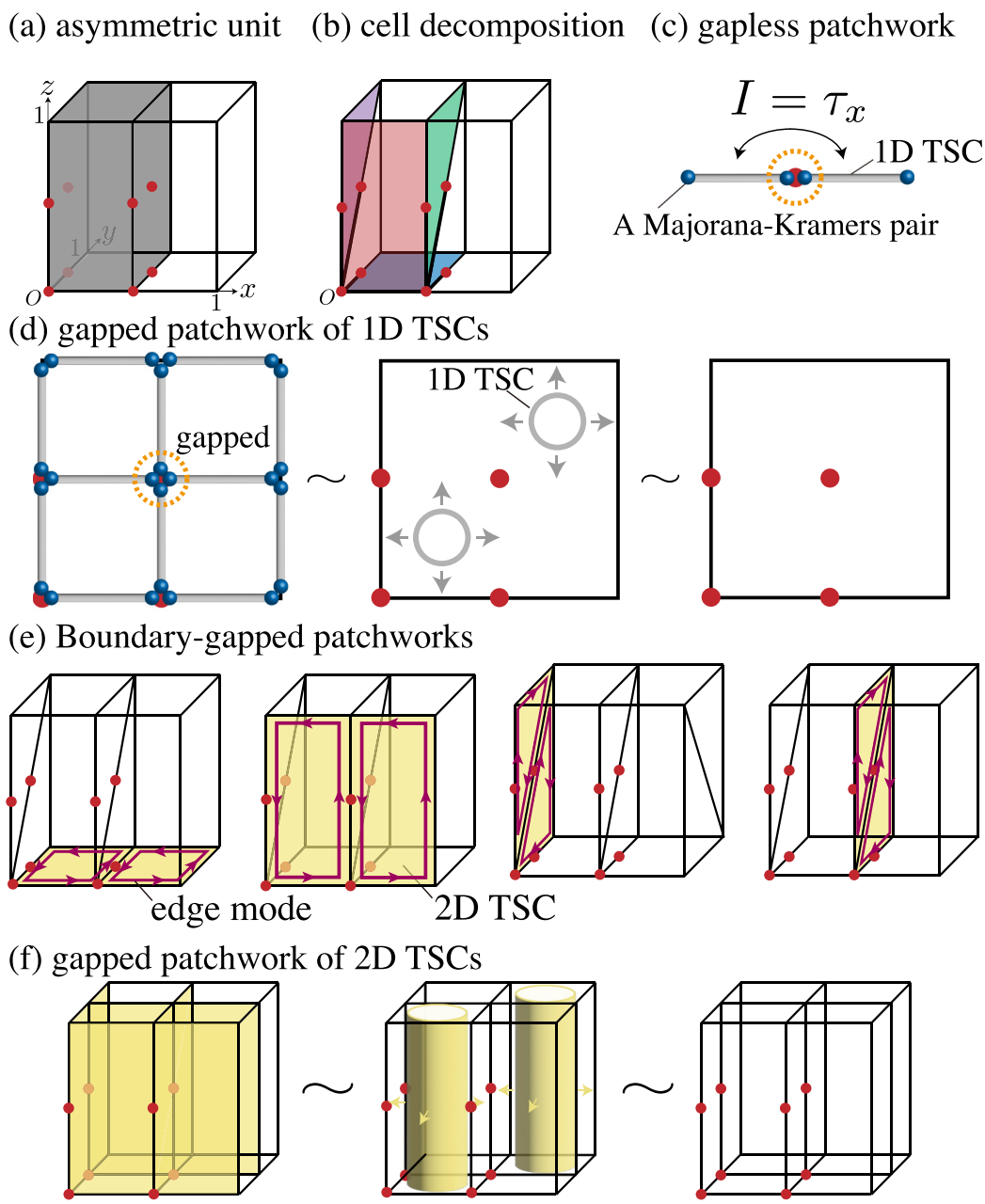

FIG. 1. Illustration of 3D patchworks in space group $P\bar{1}$. (a) A choice of asymmetric unit. (b) A cell decomposition. Symmetry-inequivalent 0-cells, 1-cells, and 2-cells are represented by red solid circles, black bold lines segments, and the colored faces, respectively. (c) An example of gapless patchworks. Here, gray lines and blue balls are 1D $\mathbb{Z}_2$-TSCs and a Kramers pair of Majorana zero modes, respectively. (d) The equivalence between a gapped patchwork constructed by 1D $\mathbb{Z}_2$-TSCs and the vacuum. (e) Boundary-gapped patchworks for the cell decomposition in (a). All yellow planes are 2D $\mathbb{Z}_2$-TSCs. (f) The equivalence between a gapped patchwork by 2D $\mathbb{Z}_2$-TSCs and the vacuum. The cell decomposition assumed in panels (d) and (f) is different from the one described in (b).

$2m-1$ ($m \in \mathbb{Z}$). Following in Refs. [69–73], we obtain the wave function of the vortex zero mode (see Appendix A for the derivation)

$$\phi^{\alpha}_{\pm,m}(r,\theta) \propto e^{-\int^{r} \frac{\mu(r')}{|\Delta_0(r')|} dr'} [u(\theta), u^*(\theta)]^T, \tag{5}$$

$$u(\theta) = e^{\frac{i}{2}(\pm\alpha+\pi/2)} e^{\pm im\theta}. \tag{6}$$

It satisfies $\tau_0 \phi^{\alpha}_{\pm,m}(r,\theta) = (-1)^m \phi^{\alpha}_{\pm,m}(r,\theta+\pi)$, which implies that the inversion eigenvalue of the vortex zero mode is $(-1)^m$. In the time-reversal symmetric case, a Kramers pair of Majorana zero modes emerges at the vortex core, whose wave functions are

$$\Phi^{\alpha}_{m,\uparrow}(r,\theta) = \phi^{\alpha}_{+,m}(r,\theta) \otimes \begin{pmatrix} 1 \\ 0 \end{pmatrix}, \tag{7}$$

$$\Phi^{\alpha}_{m,\downarrow}(r,\theta) = \phi^{-\alpha}_{-,-m}(r,\theta) \otimes \begin{pmatrix} 0 \\ 1 \end{pmatrix}. \tag{8}$$

This completes the proof.

We make the following two remarks. First, here we do not claim that every 2D time-reversal symmetric TSC with

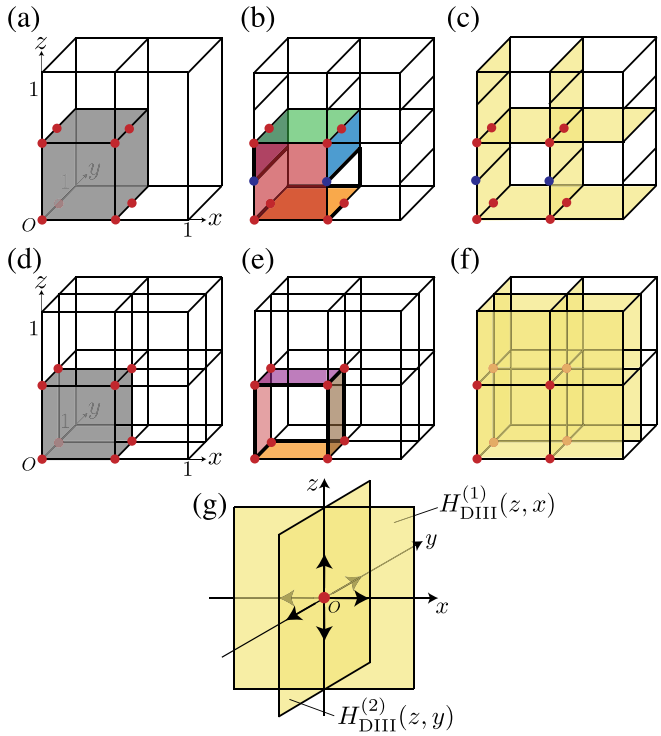

FIG. 2. Illustration of patchworks in space groups $P2/c$ and $P4/m$. (a) An asymmetric unit for space group $P2/c$. (b) A cell decomposition for $P2/c$. Colored faces are independent 2-cells; black bold line segments are symmetry-inequivalent 1-cells. Red and blue solid circles are inversion centers and rotation-invariant points, which are inequivalent 0-cells. (c) A fully gapped patchwork of $P2/c$. (d) An asymmetric unit for space group $P4/m$. (e) A cell decomposition for $P4/m$. Colored faces are independent 2-cells, black bold line segments are symmetry-inequivalent 1-cells, and red solid circles are inversion centers that are inequivalent 0-cells. (f) A boundary-gapped patchwork in $P4/m$. (g) Enlarged view of (f) near $O = (0, 0, 0)$. Black arrows represent the phase of $\Delta(\boldsymbol{r})$.

helical edge modes contains vortex zero modes. The presence or absence of vortex zero modes depends on the symmetries we strictly impose on the systems and the pairing symmetries we consider. Second, the existence of vortices is enforced only by pairing symmetries and independent of microscopic details, as seen in the above example of the even-parity inversion case. As a result, the vortex zero modes can appear in more generic time-reversal symmetric TSCs than in a TSC constructed by stacking $p_x \pm ip_y$ superconductors, when their pairing symmetries force vortices to exist in the presence of spatial symmetries. Nonetheless, the reason why here we focus on the stacking model is that it is suitable for the analytical calculations we perform in Appendix A.

Space groups $P2/c$ and $P4/m$. The patchwork in Fig. 1(f) was fully gapped but trivial. Here we discuss additional crystalline symmetries sometimes make it nontrivial or gapless due to vortex zero modes. As examples, we consider space groups $P2/c$ (No. 13) and $P4/m$ (No. 83). The configuration remains a boundary-gapped patchwork even for these space groups. Space group $P2/c$ has an additional glide symmetry, which prohibits the deformation process illustrated in Fig. 1(f) and makes this patchwork nontrivial. [See Fig. 2(c).]

In contrast, space group $P4/m$ contains fourfold rotation C_4^z along the z axis in addition to translations and inversion in $P\bar{1}$. A patchwork in Fig. 2(f) cannot be obtained from the vacuum in the presence of this symmetry. However, as shown in the following discussions, this state is gapless due to the vortex zero modes at each inversion center protected by rotation eigenvalues.

Let us focus on a neighborhood of an inversion center, for example, the one at the origin (0,0,0) [see Fig. 2(g)]. Then, the Hamiltonian is described by

$$H(\boldsymbol{r}) = \begin{pmatrix} H^{(1)}_{\mathrm{DIII}}(z,x;\Delta)\delta(y) & 0 \\ 0 & H^{(2)}_{\mathrm{DIII}}(z,y;\Delta)\delta(x) \end{pmatrix}, \tag{9}$$

$$U\left(C_4^z\right) = \begin{pmatrix} 0 & \tau_0 s_0 \\ i\tau_0 s_y & 0 \end{pmatrix}, \tag{10}$$

where $H^{(i=1,2)}_{\mathrm{DIII}}(z,x_i;\Delta) = H_{\mathrm{DIII}}[\boldsymbol{r} = (z,x_i);\Delta]$ in (4) and $U(C_4^z)$ is a unitary representation of the fourfold rotation. Note that C_4^z transforms $H^{(1)}_{\mathrm{DIII}}(z,x;\Delta)$ into $H^{(2)}_{\mathrm{DIII}}(z,y;\Delta)$ and $H^{(2)}_{\mathrm{DIII}}(z,y;\Delta)$ into $H^{(1)}_{\mathrm{DIII}}(z,-x;\Delta^*)$. The wave functions of vortex zero modes are $\Psi^{\alpha}_{m,s,1} \equiv \Phi^{\alpha}_{m,s}(r,\theta)\otimes(1,0)^T$ and $\Psi^{\alpha}_{m,s,2} \equiv \Phi^{\alpha}_{m,s}(r,\theta)\otimes(0,1)^T$, where the latter vectors describe the degree of freedom of two planes. They are transformed as

$$U\left(C_4^z\right)\left(\Psi^{\alpha}_{m,\uparrow,1}, \Psi^{\alpha}_{m,\downarrow,1}, \Psi^{\alpha}_{m,\uparrow,2}, \Psi^{\alpha}_{m,\downarrow,2}\right) = \left(\Psi^{\alpha}_{m,\uparrow,1}, \Psi^{\alpha}_{m,\downarrow,1}, \Psi^{-\alpha}_{-m,\uparrow,2}, \Psi^{-\alpha}_{-m,\downarrow,2}\right)\begin{pmatrix} 0 & 0 & 1 & 0 \\ 0 & 0 & 0 & 1 \\ 0 & 1 & 0 & 0 \\ -1 & 0 & 0 & 0 \end{pmatrix}. \tag{11}$$

This implies that the vortex zero modes have all different eigenvalues $e^{iq\frac{\pi}{4}}$ $(q = 1, 3, 5, 7)$. Hence these four Majorana-Kramers pairs cannot be gapped among them.

The same number of Majorana-Kramers pairs can be obtained by attaching two 1D TSCs along the rotation axis (z axis) such that these two interchange under inversion symmetry as illustrated in Fig 1(c). However, Majorana-Kramers pairs constructed this way have both ± 1 inversion eigenvalues. In contrast, all the four vortex zero modes have the inversion eigenvalue $(-1)^m$. Therefore, they cannot be gapped by attaching these 1D chains.

Space group $Pcc2$. It is tempting to think that such obstructions due to vortex zero modes happen only when inversion symmetry is present. However, this is untrue. Vortex zero modes can also be enforced by combinations of symmetries, not including inversion. As an example, we consider space group $Pcc2$ generated by translation along the x direction, twofold rotation along the z-axis C_{2z}, and glide G_x : $(x, y, z) \to (-x, y, z + 1/2)$.

We focus on a 2D layer at $x = 0$, which has layer group $pb2b$ (No. 30). Our cell decomposition is shown in Fig. 3(a). We introduce a 2D TSC described by (4) into each 2-cell. To respect the symmetry $U(C_{2y}) = i\tau_z s_x$ and $U(G_z) = i\tau_z s_z$, the gap function $\Delta(\boldsymbol{r})$ must satisfy $\Delta(C_{2y}\boldsymbol{r}) = \Delta^*(\boldsymbol{r})$ and $\Delta(G_z\boldsymbol{r}) = -\Delta(\boldsymbol{r})$, which implies the presence of vortices with odd-integer winding. We additionally require that all zero

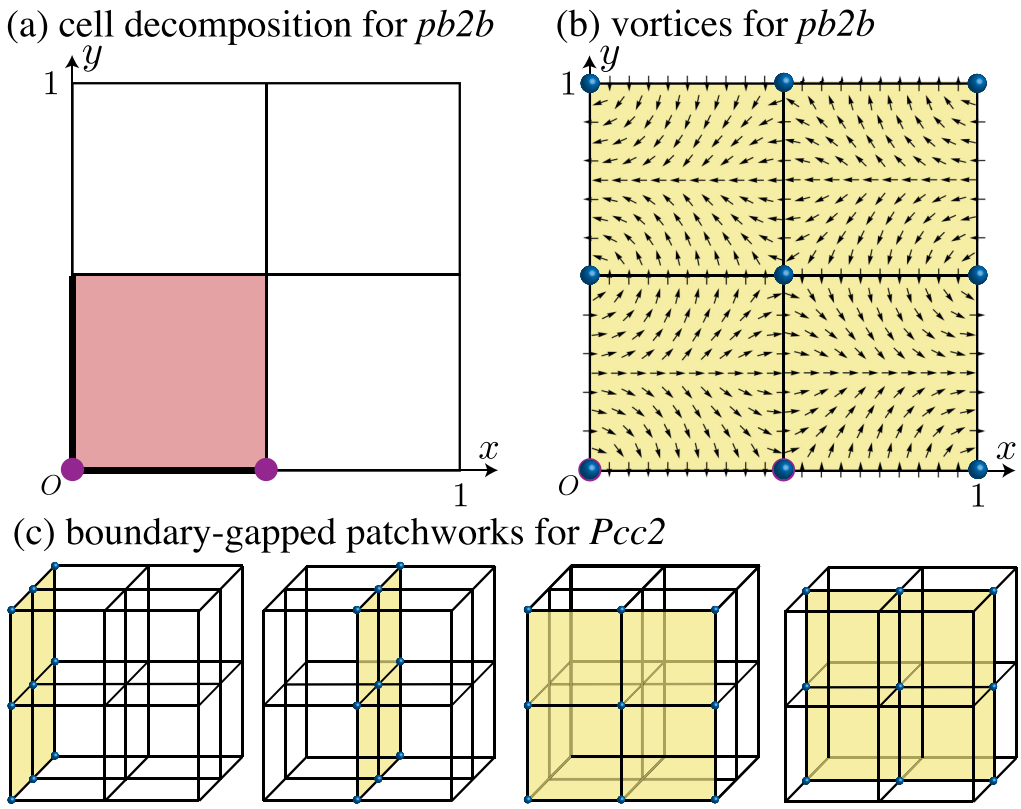

FIG. 3. Illustration of patchworks in space group *Pcc*2. (a) A cell decomposition for layer group *pb2b*. Symmetry-inequivalent 0-cells, 1-cells, and 2-cells are represented by solid circles, black bold line segments, and the colored face, respectively. (b) An example of vortex configuration for *pb2b*. A vortex emerge at each of the 0-cells (blue balls). Arrows represent the phase of $\Delta(\boldsymbol{r})$. (c) Boundary-gapped patchworks for space group *Pcc*2. Note that each plane is symmetric under symmetries in *pb2b*.

modes can exist only at 0-cells. An example of configurations satisfying all of these requirements is shown in Fig. 3(b). Therefore, all the four boundary-gapped patchworks for space group *Pcc*2 in Fig. 3(c) have vortex zero modes. A fully gapped patchwork can be constructed by stacking these four, which results in $E^{\infty}_{2,-2} = \mathbb{Z}_2$. Vortices can also be enforced in 2D systems with other layer group symmetries, e.g., $pm2_1b$ (No. 28).

B. Results for other crystalline symmetries

Applying the above discussions to various symmetry settings, we obtain fully gapped patchworks $E^{\infty}_{2,-2}$ in all rod groups, layer groups, and space groups with conventional pairing symmetries. In the Supplemental Material [74], we provide lists of (i) $E^{\infty}_{p,-p}$, (ii) a cell decomposition, and (iii) patchworks that correspond to generators of $E^{\infty}_{1,-1}$ and $E^{\infty}_{2,-2}$ for each space group. We also include $E^{\infty}_{p,-p}$ for rod and layer groups.

Here, we explain how to utilize these results through an example of space group $P\bar{3}$ (No. 147). This space group is symmorphic and centrosymmetric, which is generated by inversion, threefold rotation, and lattice translations. Nevertheless, there exists a topological superconducting phase with conventional pairing symmetry. In Figs. 4(a) and 4(b), we show an asymmetric unit used in this work and a part of the cell decomposition. Symmetry-inequivalent 0-cells are labeled by uppercase alphabets $A, B, C, \ldots$, 1-cells are labeled by lowercase alphabets $a, b, c, \ldots$, and 2-cells are labeled by lowercase Greek letters. Their coordinates are given in the Supplemental Material [74]. For this space group, we find $E^{\infty}_{1,-1} = \mathbb{Z}$ and $E^{\infty}_{2,-2} = 0$. The patchwork generating $E^{\infty}_{1,-1}$ is shown in Fig. 4(c), where 1D $\mathbb{Z}$-TSCs are placed on 1-cells a and b in a symmetric manner.

These pieces of information are useful to understand the boundary signature of this phase. For example, let us focus on the boundary perpendicular to the z axis by imposing the open boundary condition on the z direction and the periodic boundary condition on the other two directions. Based on the real-space picture in Fig. 4(c), we expect that Dirac surface states originate from the Majorana zero modes at the edge of each 1D chain. We numerically confirm this using a tight-binding model illustrated in Fig. 5(a), whose boundary state is shown in Fig. 5(b) (see Appendix B for more details).

C. Final classification

As discussed in overview, we have to solve the group extension problem to obtain the final classification. In our problem, we have to find an Abelian group X that satisfies

$$X/E^{\infty}_{1,-1} \simeq E^{\infty}_{2,-2}. \tag{12}$$

There can be multiple possibilities but the correct one can be identified by a physical argument. We analyze mass terms of the Dirac Hamiltonian that describes the phase obtained by stacking two copies of a generator of $E^{\infty}_{2,-2}$. The group

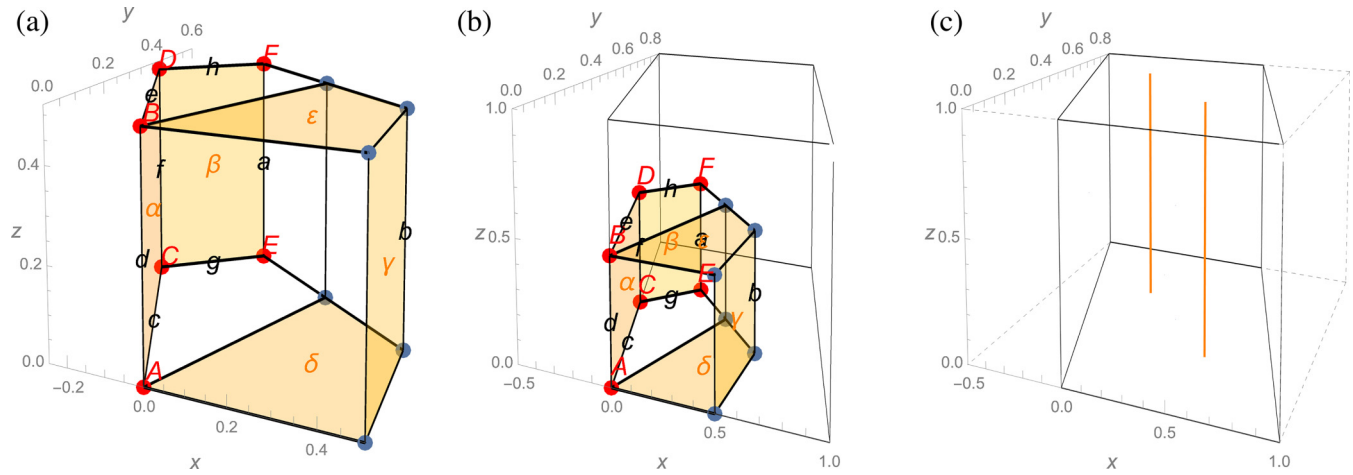

FIG. 4. Summary of results for space group $P\bar{3}$. (a) An asymmetric unit for space group $P\bar{3}$. A cell decomposition used in this work is partially shown. Labels of symmetry-inequivalent p-cells ($p = 0,\ 1$, and 2) are defined in the Supplemental Material. (b) An asymmetric unit with the unit cell. (c) The patchwork generating $E^{\infty}_{1,-1}$. Here, orange lines represent 1D $\mathbb{Z}$-TSCs.

extension is trivial if the uniform mass is allowed in the Dirac Hamiltonian; otherwise, it is nontrivial. Given X, the final classification is given by $X \oplus E^{\infty}_{3,-3}$.

To demonstrate how to solve (12), here we discuss layer group pb as an example. This group is generated by glide symmetry $G_x : (x, y, z) \to (-x, y + 1/2, z)$ in addition to translation in y. After performing the real-space classification, we obtain $E^{\infty}_{1,-1} = (\mathbb{Z}_2)^2$ and $E^{\infty}_{2,-2} = \mathbb{Z}_2$. Their generators are illustrated in Fig. 6(a). The generator of $E^{\infty}_{2,-2}$ is described by the Dirac Hamiltonian (4) with a constant $\Delta(\boldsymbol{r})$. Then, we ask if the patchwork constructed by stacking two copies of the generator of $E^{\infty}_{2,-2}$ is a nontrivial element of $E^{\infty}_{1,-1}$. By analyzing the mass term, we find that the stacked patchwork is still nontrivial and it falls into $(0, 1) \in E^{\infty}_{1,-1} = (\mathbb{Z}_2)^2$. This result indicates that the group extension is nontrivial and that the final classification is $\mathbb{Z}_2 \times \mathbb{Z}_4$ (see the Supplemental Material for more details [74]).

Another class of examples is layer group pn ($n = 2, 4, 6$), which contains n-fold rotation symmetry. From the real-space classification, we have $E^{\infty}_{1,-1} = (\mathbb{Z}_2)^{4-n/2}$ and $E^{\infty}_{2,-2} = \mathbb{Z}_2$. Unlike the case of layer group pb, the group extension is trivial and the final classification is $E^{\infty}_{1,-1} \oplus E^{\infty}_{2,-2} = (\mathbb{Z}_2)^{5-n/2}$ (see the Supplemental Material for more details [74]).

The one-by-one analysis of mass terms is laborious. However, for 159 out of 230 space groups, we succeeded in sidestepping this issue by computing the final classification using AHSS in momentum space [54]. It should be emphasized that the real-space classifications are still crucial even when the momentum space classifications are available. This is because the classifications in momentum space are not usually informative on the nature of the boundary modes in each entry of the classification. In the Supplemental Material,

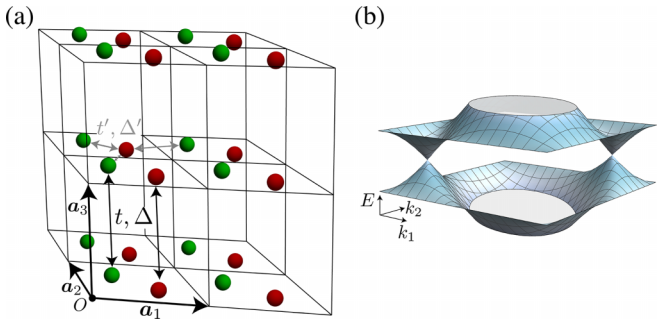

FIG. 5. Illustration of the tight-binding model in space group $P\bar{3}$. (a) Real-space description of the tight-binding model. There are two orbital degrees of freedom in the unit cell. Primitive lattice vectors are $\boldsymbol{a}_1 = (1, 0, 0)^T$, $\boldsymbol{a}_2 = (-1/2, \sqrt{3}/2, 0)^T$, and $\boldsymbol{a}_3 = (0, 0, 1)^T$, and sites are defined on $(2/3 + R_1)\boldsymbol{a}_1 + (1/3 + R_2)\boldsymbol{a}_2 + R_3\boldsymbol{a}_3$ and $(1/3 + R_1)\boldsymbol{a}_1 + (2/3 + R_2)\boldsymbol{a}_2 + R_3\boldsymbol{a}_3$ [$R_1, R_2, R_3 \in \mathbb{Z}$]. Here, t and Δ denote parameters for hopping and pairing between the same orbitals along the z direction and t' and Δ' represent the nearest hopping and pairing between the two different orbitals. (b) Energy spectrum of the surface states of the tight-binding model defined in Appendix B. Here, the open boundary condition is imposed on the z direction and the periodic one is on the other directions. The parameters are $t = 1.2$, $\Delta = 1$, $\mu = 1$, $t' = 0.2$, and $\Delta' = 0.1$.

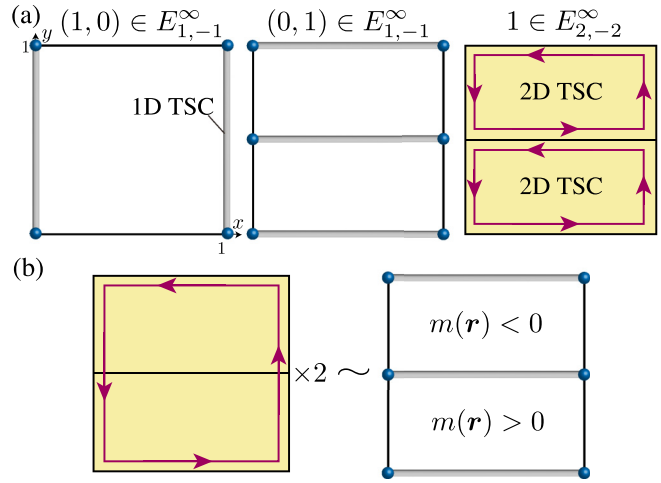

FIG. 6. Illustration of the group extension problem in pb. (a) All boundary-gapped patchworks, which are generators of $E^{\infty}_{1,-1}$ and $E^{\infty}_{2,-2}$. (b) Relation between the stacked 2D $\mathbb{Z}_2$-TSCs and a boundary-gapped patchwork composed of 1D $\mathbb{Z}_2$-TSCs. Here, $m(\boldsymbol{r})$ denotes the mass that will partially gap out the edge states.

we also show the final classifications for all rod groups, all layer groups, and 159 space groups.

IV. DISCUSSION

In this work, by analyzing the wave functions of vortex zero modes and studying their symmetry representations, we succeeded in deriving obstructions to constructing gapped phases of superconductors. This enabled us to systematically perform the real-space classification for superconductors with conventional pairing symmetries in all rod, layer, and space groups. We found that topologically nontrivial superconducting phases exist in 199 out of 230 space groups (61 centrosymmetric and 138 noncentrosymmetric space groups). In addition, our results for all rod groups and layer groups are complete K-theoretic classifications. 159 space groups are also complete. We leave the group extension problem in the remaining 71 space groups as future work. Our work opens up a direction of the material search focusing on the conventional pairing symmetries that are the majority in real materials.

It should be noted that the conventional s-wave pairing may not be sufficient to realize topological phases found in this work; it might be that sign-changing gap functions, known as extended s or $s_\pm$ wave, are required. Such pairings are still classified as "conventional" from the viewpoint of pairing symmetries. Indeed, in all of our examples, TSCs used as building blocks require such sign-changing pairings [50,51]. Given this observation, we conjecture that this is in fact the case, but we leave a detailed study on the necessary conditions as a future work.

Note added. Recently, Ref. [75] appeared, which is based on a similar idea and discusses 2D topological crystalline phases constructed only by 1D TSCs in wallpaper groups.

ACKNOWLEDGMENTS

We thank H. C. Po for invaluable discussions in previous collaborations. S.O. was supported by the ANRI Fellowship and KAKENHI Grant No. JP20J21692 from the Japan Society for the Promotion of Science (JSPS). K.S. was supported by JST CREST Grant No. JPMJCR19T2 and JST PRESTO Grant No. JPMJPR18L4. H.W. was supported by JST PRESTO Grant No. JPMJPR18LA and JSPS KAKENHI Grants No. JP20H01825 and No. JP21H01789.

APPENDIX A: VORTEX ZERO MODES IN TWO-DIMENSIONAL TOPOLOGICAL SUPERCONDUCTORS

In this Appendix, we provide more detailed discussions on vortex zero modes in two-dimensional topological superconductors.

1. $p_x \pm ip_y$ superconductor

Following Refs. [22,69,73], here we show that a vortex with an odd-integer winding in $p_x \pm ip_y$ superconductors traps a vortex zero mode. To this end, we discuss the eigenvalue equation $H_\pm(\boldsymbol{r};\Delta)\phi(\boldsymbol{r}) = E\phi(\boldsymbol{r})$ for the continuum model in (3). As discussed in Ref. [69], a vortex is realized as a small circular edge between the trivial phase inside and the bulk $p_x \pm ip_y$ superconductor outside. In the polar coordinate (r,θ), the off-diagonal component of the matrix in (3) is rewritten as

$$\Delta(\boldsymbol{r})\left(\frac{1}{i}\partial_x \pm i\frac{1}{i}\partial_y\right) = \Delta(\boldsymbol{r})e^{\pm i\theta}\left(\frac{1}{i}\partial_r \pm i\frac{1}{r}\frac{1}{i}\partial_\theta\right). \tag{A1}$$

Furthermore, in the diagonal component, we assume that $\mu(\boldsymbol{r}) = \mu(r)$ such that $\mu(r) \to \mu_0 > 0$ as $r \to \infty$ and $\mu(r) \to -\mu_0$ as $r \to 0$. Then, the kinetic term $-\nabla^2/2m$ is omitted:

$$-\frac{\nabla^2}{2m} - \mu(\boldsymbol{r}) \simeq -\mu(r). \tag{A2}$$

Then, the eigenvalue equation is rewritten as

$$(H_0 + V)\begin{pmatrix} u \\ u^* \end{pmatrix} = E\begin{pmatrix} u \\ u^* \end{pmatrix}, \tag{A3}$$

$$H_0 = \begin{pmatrix} -\mu(\boldsymbol{r}) & -i\Delta(\boldsymbol{r})e^{\pm i\theta}\partial_r \\ -i\Delta^*(\boldsymbol{r})e^{\mp i\theta}\partial_r & \mu(\boldsymbol{r}) \end{pmatrix}, \tag{A4}$$

$$V = \begin{pmatrix} 0 & \pm i\Delta(\boldsymbol{r})e^{\pm i\theta}\frac{1}{r}\frac{1}{i}\partial_\theta \\ \mp i\Delta^*(\boldsymbol{r})e^{\mp i\theta}\frac{1}{r}\frac{1}{i}\partial_\theta & 0 \end{pmatrix}. \tag{A5}$$

Here we used PHS to relate the first and second component of the eigenvector. When the winding number of the vortex (vorticity) is n, we set $\Delta(\boldsymbol{r}) = |\Delta_0(r)|e^{\pm i(\alpha+n\theta)}$.

In the following, we first ignore the second term V in (A3) and derive the zero-energy solution for the simplified equation. When the second term V is ignored, Eq. (A3) is simplified as

$$-\mu(r)u - i|\Delta_0(r)|e^{\pm i(\alpha+n\theta)}e^{\pm i\theta}\partial_r u^* = Eu. \tag{A6}$$

By the gauge transformation $\tilde{u} = e^{\mp im\theta}u$, this equation can be rewritten as

$$-\mu(r)\tilde{u} - i|\Delta_0(r)|e^{\pm i[\alpha+(n-2m)\theta]}e^{\pm i\theta}\partial_r\tilde{u}^* = E\tilde{u}, \tag{A7}$$

which is equivalent to the equation for a vortex with winding $(n-2m)$. Therefore, the vorticity n can be changed by an even number $2m$. This indicates that, when n is even, Eq. (A7) becomes the equation without nontrivial winding (i.e., $n = 0$), for which we know the spectrum is gapped. Thus Eq. (A6) does not have any zero-energy solution.

On the other hand, when $n = 2m-1$, we explicitly find a zero-energy solution to (A6) [22]:

$$\phi_{\pm,m}(r,\theta) \propto \begin{pmatrix} e^{\frac{i}{2}(\pm\alpha+\pi/2)}e^{\pm im\theta} \\ e^{-\frac{i}{2}(\pm\alpha+\pi/2)}e^{\mp im\theta} \end{pmatrix} e^{-\int^r \frac{\mu(r')}{|\Delta_0(r')|}dr'}. \tag{A8}$$

Next, we claim that the zero-energy solution persists in the presence of the second term V in (A3). To see this, we introduce a parameter $\epsilon \in [0,1]$ and consider the Hamiltonian

$$(H_0 + \epsilon V)\phi(\epsilon,\boldsymbol{r}) = E(\epsilon)\phi(\epsilon,\boldsymbol{r}). \tag{A9}$$

According to the first-order perturbation theory, $\partial_\epsilon E(\epsilon)$ is given by $\phi(\epsilon,\boldsymbol{r})^\dagger V\phi(\epsilon,\boldsymbol{r})$, which vanishes due to PHS. Likewise, any topological property does not change as we increase ϵ from 0 to 1 [73]. Thus we always use the wave function $\phi_{\pm,m}(r,\theta)$ in (A8) in the following discussions.

TABLE I. Summary of representations and transformations of $\Delta(\boldsymbol{r})$.

g	$U(g)$	Transformation of $\Delta(\boldsymbol{r})$	$\Delta(\boldsymbol{r})$ at $g\boldsymbol{r}=\boldsymbol{r}$
I	$\tau_0 s_0$	$\Delta(-\boldsymbol{r})=-\Delta(\boldsymbol{r})$	0
C_n^z	$e^{i\frac{\pi}{n}\tau_z s_z}$	$\Delta(C_n^z\boldsymbol{r})=\Delta(\boldsymbol{r})$	Arbitrary
C_2^x	$i\tau_0 s_y$	$\Delta(C_2^x\boldsymbol{r})=\Delta^*(\boldsymbol{r})$	Real

TABLE II. Summary of representations of vortex zero modes for symmetries in Table I.

g	$g(\theta)$	$U_{\text{vortex}}(g)$
I	$\theta+\pi$	$(-1)^m\sigma_0$
C_n^z	$\theta+\frac{2\pi}{n}$	$\cos\frac{(2m-1)\pi}{n}\sigma_0$
C_2^x	$-\theta$	$\cos\alpha\, i\sigma_y$

2. Time-reversal symmetric topological superconductors

As discussed in the main text, the representations of vortex zero modes play a crucial role in the real-space classifications. Here, we discuss the symmetry representations of vortex zero modes. We first find symmetry representations of $H_{\text{DIII}}(\boldsymbol{r};\Delta)$ in (4) and then we obtain representations of vortex zero modes.

In the following, we consider that the 2D TSC is defined on the xy plane. Also, we assume the conventional pairing symmetry. Symmetry operations, which keep a plane invariant, are generated by combinations of inversion I, n-fold rotation along z-axis C_n^z, and twofold rotation along x-axis C_2^x. Let us start with inversion symmetry. Inversion symmetry is represented by $U(I)=\tau_0 s_0$, which is encoded in the model as

$$U(I)H_{\text{DIII}}(\boldsymbol{r};\Delta)=H_{\text{DIII}}(-\boldsymbol{r};-\Delta)U(I), \tag{A10}$$

implying that $\Delta(-\boldsymbol{r})=-\Delta(\boldsymbol{r})$. This means that the vorticity n is odd. That is, inversion symmetry enforces the emergence of a vortex zero mode.

Similarly, n-fold rotation symmetry $(n=2,3,4,6)$ is given by $U(C_n^z)=e^{i\frac{\pi}{n}\tau_z s_z}$, which satisfies

$$U\left(C_n^z\right)H_{\text{DIII}}(\boldsymbol{r};\Delta)=H_{\text{DIII}}\left(C_n^z\boldsymbol{r};\Delta\right)U\left(C_n^z\right). \tag{A11}$$

This time, we have $\Delta(C_n^z\boldsymbol{r})=\Delta(\boldsymbol{r})$. Thus the winding is even when the n-fold rotation $U(C_n^z)$ $(n=2,4,6)$ exists. Therefore, inversion and these rotations do not coexist.

As for C_2^x, symmetry representation is expressed by

$$U\left(C_2^x\right)=\begin{pmatrix}0 & \tau_0\\ -\tau_0 & 0\end{pmatrix}=i\tau_0 s_y \tag{A12}$$

such that

$$U(C_2^x)H_{\text{DIII}}(\boldsymbol{r};\Delta)=H_{\text{DIII}}(C_2^x\boldsymbol{r};\Delta^*)U(C_2^x). \tag{A13}$$

This implies that $\Delta(C_2^x\boldsymbol{r})=\Delta^*(\boldsymbol{r})$.

Symmetry representations of other symmetries are constructed by I, C_n^z, and C_2^x. For example, twofold rotation symmetry along the y axis (denoted by $C_2^y=C_2^zC_2^x$) is defined by $U(C_2^y)\equiv U(C_2^z)U(C_2^x)$. Then, $\Delta(C_2^y\boldsymbol{r})=\Delta^*(\boldsymbol{r})$. We summarize the representations and transformations of $\Delta(\boldsymbol{r})$ for all symmetries in Table I.

Finally, we discuss how wave functions of vortex zero modes in Eqs. (7) and (8) are transformed under symmetry g in Table I. We find

$$\begin{aligned}&U(g)[\Phi_{m,\uparrow}(r,\theta),\Phi_{m,\downarrow}(r,\theta)]\\&\quad=[\Phi_{m,\uparrow}(r,g(\theta)),\Phi_{m,\downarrow}(r,g(\theta))]U_{\text{vortex}}(g),\end{aligned} \tag{A14}$$

where $g(\theta)$ is the angle after the transformation by g. For example, $I(\theta)=\theta+\pi$. In Table II, we tabulate $g(\theta)$ and $U_{\text{vortex}}(g)$ for symmetries in Table I.

APPENDIX B: TIGHT-BINDING MODEL FOR A GENERATOR OF $E^{\infty}_{\mathbf{1},-\mathbf{1}}$ IN $P\bar{3}$

Here, we provide the tight-binding model that we used in Fig. 5. According to the patchwork in Fig. 4, 1D $\mathbb{Z}$-TSCs are placed on threefold rotation symmetric lines $(2/3+R_1)\boldsymbol{a}_1+(1/3+R_2)\boldsymbol{a}_2+z\boldsymbol{a}_3$ and $(1/3+R_1)\boldsymbol{a}_2+(2/3+R_2)\boldsymbol{a}_2+z\boldsymbol{a}_3$ $[R_1,R_2\in\mathbb{Z}]$, where $\boldsymbol{a}_1=(1,0,0)^T$, $\boldsymbol{a}_2=(-1/2,\sqrt{3}/2,0)^T$, and $\boldsymbol{a}_3=(0,0,1)^T$. The Hamiltonians of each 1D $\mathbb{Z}$-TSC are given by

$$\begin{aligned}\hat{H}_a=\sum_{\boldsymbol{R}}\Bigg[&-t\sum_{s=\uparrow,\downarrow}\{(c^\dagger_{\boldsymbol{R}+\boldsymbol{a}_z,a,s}c_{\boldsymbol{R},a,s})+\text{H.c.}\}\\&+\sum_{s=\uparrow,\downarrow}+2(t-\mu)c^\dagger_{\boldsymbol{R},a,s}c_{\boldsymbol{R},a,s}\\&+\frac{\Delta}{i}(c^\dagger_{\boldsymbol{R}+\boldsymbol{a}_z,a,\uparrow}c^\dagger_{\boldsymbol{R},a,\downarrow}-c^\dagger_{\boldsymbol{R},a,\uparrow}c^\dagger_{\boldsymbol{R}+\boldsymbol{a}_z,a,\downarrow})+\text{H.c.}\Bigg],\end{aligned} \tag{B1}$$

$$\hat{H}_b=\hat{I}\hat{H}_a\hat{I}^{-1}, \tag{B2}$$

where a and b denote two orbital degrees of freedom corresponding to two 1D TSCs in the unit cell. Inversion I interchanges creation operators of two orbital degrees of freedom, i.e., $c^\dagger_{\boldsymbol{R},b,s}=\hat{I}c^\dagger_{-\boldsymbol{R}-\boldsymbol{a}_1-\boldsymbol{a}_2,a,s}\hat{I}^{-1}$. Also, the threefold rotation C_3^z transforms the creation operators as $\hat{C}_3^z c^\dagger_{\boldsymbol{R},a,s}[\hat{C}_3^z]^{-1}=e^{i\frac{\pi}{3}s}c^\dagger_{C_3^z\boldsymbol{R}-\boldsymbol{a}_1,a,s}$ and $\hat{C}_3^z c^\dagger_{\boldsymbol{R},b,s}[\hat{C}_3^z]^{-1}=e^{i\frac{\pi}{3}s}c^\dagger_{C_3^z\boldsymbol{R}-\boldsymbol{a}_1-\boldsymbol{a}_2,b,s}$.

In momentum space, the Hamiltonian is expressed by $\hat{H}=\boldsymbol{\psi}^\dagger_{\boldsymbol{k}}H^{\text{BdG}}_{\boldsymbol{k}}\boldsymbol{\psi}_{\boldsymbol{k}}$, where

$$\boldsymbol{\psi}^\dagger_{\boldsymbol{k}}=(c^\dagger_{\boldsymbol{k},a,\uparrow}c^\dagger_{\boldsymbol{k},a,\downarrow}c_{-\boldsymbol{k},a,\uparrow}c_{-\boldsymbol{k},a,\downarrow}c^\dagger_{\boldsymbol{k},b,\uparrow}c^\dagger_{\boldsymbol{k},b,\downarrow}c_{-\boldsymbol{k},b,\uparrow}c_{-\boldsymbol{k},b,\downarrow}), \tag{B3}$$

$$H^{\text{BdG}}_{\boldsymbol{k}}=\begin{pmatrix}H^{\text{BdG}}_{\boldsymbol{k},a} & w_{\boldsymbol{k}}V\\ w^*_{\boldsymbol{k}}V^\dagger & H^{\text{BdG}}_{\boldsymbol{k},b}\end{pmatrix}, \tag{B4}$$

$$H^{\text{BdG}}_{\boldsymbol{k},a}=[t(1-\cos k_z)-\mu]\tau_z s_0+\Delta\,\sin k_z\tau_x s_x, \tag{B5}$$

$$H^{\text{BdG}}_{\boldsymbol{k},b}=[t(1-\cos k_z)-\mu]\tau_z s_0-\Delta\,\sin k_z\tau_x s_x, \tag{B6}$$

$$V=\begin{pmatrix}-t' & 0 & 0 & -\Delta'\\ 0 & -t' & \Delta' & 0\\ 0 & \Delta' & t' & 0\\ -\Delta' & 0 & 0 & t'\end{pmatrix}, \tag{B7}$$

$$w_{\boldsymbol{k}}=1+e^{i2\pi k_1}+e^{-i2\pi k_2}. \tag{B8}$$

Diagonal parts denote inter-layer hopping and pairing between the same orbital, and off-diagonal parts represent the hopping and pairing between the two orbital degrees of freedom in unit cell. In our numerical simulations, we used parameters $(t,\mu,\Delta,t',\Delta')=(1.2,1.0,1.0,0.2,0.1)$.

We find the following symmetry representations of $H_{\boldsymbol{k}}^{\mathrm{BdG}}$:

$$U_{\boldsymbol{k}}^{\mathrm{BdG}}(I) = e^{i2\pi(k_1+k_2)}\begin{pmatrix} 0 & \tau_0 s_0 \\ \tau_0 s_0 & 0 \end{pmatrix}, \tag{B9}$$

$$U_{\boldsymbol{k}}^{\mathrm{BdG}}(C_3^z) = \begin{pmatrix} e^{i2\pi(k_1+k_2)}e^{i\frac{\pi}{3}\tau_z s_z} & 0 \\ 0 & e^{i2\pi k_2}e^{i\frac{\pi}{3}\tau_z s_z} \end{pmatrix}, \tag{B10}$$

$$U(\mathcal{C}) = \begin{pmatrix} \tau_x s_0 & 0 \\ 0 & \tau_x s_0 \end{pmatrix}, \tag{B11}$$

$$U(\mathcal{T}) = \begin{pmatrix} i\tau_0 s_y & 0 \\ 0 & i\tau_0 s_y \end{pmatrix}. \tag{B12}$$

[1] S. R. Elliott and M. Franz, Colloquium: Majorana fermions in nuclear, particle, and solid-state physics, Rev. Mod. Phys. **87**, 137 (2015).

[2] A. P. Schnyder, S. Ryu, A. Furusaki, and A. W. W. Ludwig, Classification of topological insulators and superconductors in three spatial dimensions, Phys. Rev. B **78**, 195125 (2008).

[3] A. Kitaev, Periodic table for topological insulators and superconductors, *Advances in Theoretical Physics: Landau Memorial Conference*, AIP Conf. Proc. No. 1134 (AIP, Melville, NY, 2009), p. 22.

[4] S. Ryu, A. P. Schnyder, A. Furusaki, and A. W. W. Ludwig, Topological insulators and superconductors: Tenfold way and dimensional hierarchy, New J. Phys. **12**, 065010 (2010).

[5] M. Sigrist and K. Ueda, Phenomenological theory of unconventional superconductivity, Rev. Mod. Phys. **63**, 239 (1991).

[6] M. H. Fischer, T. Neupert, C. Platt, A. P. Schnyder, W. Hanke, J. Goryo, R. Thomale, and M. Sigrist, Chiral d-wave superconductivity in SrPtAs, Phys. Rev. B **89**, 020509(R) (2014).

[7] L. Fu, Odd-parity topological superconductor with nematic order: Application to Cu_x Bi_2 Se_3, Phys. Rev. B **90**, 100509(R) (2014).

[8] S. Sasaki, M. Kriener, K. Segawa, K. Yada, Y. Tanaka, M. Sato, and Y. Ando, Topological superconductivity in $Cu_xBi_2Se_3$, Phys. Rev. Lett. **107**, 217001 (2011).

[9] Y. Yanase and K. Shiozaki, Möbius topological superconductivity in UPt_3, Phys. Rev. B **95**, 224514 (2017).

[10] T. Kawakami, T. Okamura, S. Kobayashi, and M. Sato, Topological crystalline materials of $J = 3/2$ electrons: Antiperovskites, dirac points, and high winding topological superconductivity, Phys. Rev. X **8**, 041026 (2018).

[11] A. Daido, T. Yoshida, and Y. Yanase, $\mathbb{Z}_4$ topological superconductivity in UCoGe, Phys. Rev. Lett. **122**, 227001 (2019).

[12] J. Ishizuka, S. Sumita, A. Daido, and Y. Yanase, Insulator-metal transition and topological superconductivity in UTe_2 from a first-principles calculation, Phys. Rev. Lett. **123**, 217001 (2019).

[13] T. Shang, M. Smidman, A. Wang, L.-J. Chang, C. Baines, M. K. Lee, Z. Y. Nie, G. M. Pang, W. Xie, W. B. Jiang, M. Shi, M. Medarde, T. Shiroka, and H. Q. Yuan, Simultaneous nodal superconductivity and time-reversal symmetry breaking in the noncentrosymmetric superconductor CaPtAs, Phys. Rev. Lett. **124**, 207001 (2020).

[14] Y.-T. Hsu, W. S. Cole, R.-X. Zhang, and J. D. Sau, Inversion-protected higher-order topological superconductivity in monolayer WTe_2, Phys. Rev. Lett. **125**, 097001 (2020).

[15] K. Nogaki, A. Daido, J. Ishizuka, and Y. Yanase, Topological crystalline superconductivity in locally noncentrosymmetric $CeRh_2As_2$, Phys. Rev. Res. **3**, L032071 (2021).

[16] F. Tang, S. Ono, X. Wan, and H. Watanabe, High-throughput investigations of topological and nodal superconductors, Phys. Rev. Lett. **129**, 027001 (2022).

[17] M. Sato, Topological odd-parity superconductors, Phys. Rev. B **81**, 220504(R) (2010).

[18] L. Fu and E. Berg, Odd-parity topological superconductors: theory and application to $Cu_xBi_2Se_3$, Phys. Rev. Lett. **105**, 097001 (2010).

[19] M. Sato, Topological properties of spin-triplet superconductors and Fermi surface topology in the normal state, Phys. Rev. B **79**, 214526 (2009).

[20] Y. Ueno, A. Yamakage, Y. Tanaka, and M. Sato, Symmetry-protected majorana fermions in topological crystalline superconductors: Theory and application to Sr_2RuO_4, Phys. Rev. Lett. **111**, 087002 (2013).

[21] K. Shiozaki and M. Sato, Topology of crystalline insulators and superconductors, Phys. Rev. B **90**, 165114 (2014).

[22] M. Sato and S. Fujimoto, Majorana fermions and topology in superconductors, J. Phys. Soc. Jpn. **85**, 072001 (2016).

[23] K. Shiozaki, M. Sato, and K. Gomi, Topological crystalline materials: General formulation, module structure, and wallpaper groups, Phys. Rev. B **95**, 235425 (2017).

[24] J. Langbehn, Y. Peng, L. Trifunovic, F. von Oppen, and P. W. Brouwer, Reflection-symmetric second-order topological insulators and superconductors, Phys. Rev. Lett. **119**, 246401 (2017).

[25] E. Khalaf, Higher-order topological insulators and superconductors protected by inversion symmetry, Phys. Rev. B **97**, 205136 (2018).

[26] M. Geier, L. Trifunovic, M. Hoskam, and P. W. Brouwer, Second-order topological insulators and superconductors with an order-two crystalline symmetry, Phys. Rev. B **97**, 205135 (2018).

[27] S. Ono and H. Watanabe, Unified understanding of symmetry indicators for all internal symmetry classes, Phys. Rev. B **98**, 115150 (2018).

[28] L. Trifunovic and P. W. Brouwer, Higher-order bulk-boundary correspondence for topological crystalline phases, Phys. Rev. X **9**, 011012 (2019).

[29] E. Cornfeld and A. Chapman, Classification of crystalline topological insulators and superconductors with point group symmetries, Phys. Rev. B **99**, 075105 (2019).

[30] S. Ono, Y. Yanase, and H. Watanabe, Symmetry indicators for topological superconductors, Phys. Rev. Res. **1**, 013012 (2019).

[31] A. Skurativska, T. Neupert, and M. H. Fischer, Atomic limit and inversion-symmetry indicators for topological superconductors, Phys. Rev. Res. **2**, 013064 (2020).

[32] S. Ono, H. C. Po, and H. Watanabe, Refined symmetry indicators for topological superconductors in all space groups, Sci. Adv. **6**, eaaz8367 (2020).

[33] J. Ahn and B.-J. Yang, Higher-order topological superconductivity of spin-polarized fermions, Phys. Rev. Res. **2**, 012060(R) (2020).

[34] M. Geier, P. W. Brouwer, and L. Trifunovic, Symmetry-based indicators for topological Bogoliubov–de Gennes Hamiltonians, Phys. Rev. B **101**, 245128 (2020).

[35] A. Tiwari, A. Jahin, and Y. Wang, Chiral dirac superconductors: Second-order and boundary-obstructed topology, Phys. Rev. Res. **2**, 043300 (2020).

[36] S. Ono, H. C. Po, and K. Shiozaki, $\mathbb{Z}_2$-enriched symmetry indicators for topological superconductors in the 1651 magnetic space groups, Phys. Rev. Res. **3**, 023086 (2021).

[37] S.-J. Huang and Y.-T. Hsu, Faithful derivation of symmetry indicators: A case study for topological superconductors with time-reversal and inversion symmetries, Phys. Rev. Res. **3**, 013243 (2021).

[38] E. Cornfeld and S. Carmeli, Tenfold topology of crystals: Unified classification of crystalline topological insulators and superconductors, Phys. Rev. Res. **3**, 013052 (2021).

[39] S. Ono and K. Shiozaki, Symmetry-based approach to superconducting nodes: unification of compatibility conditions and gapless point classifications, Phys. Rev. X **12**, 011021 (2022).

[40] Y. Chen, S.-J. Huang, Y.-T. Hsu, and T.-C. Wei, Topological invariants beyond symmetry indicators: Boundary diagnostics for twofold rotationally symmetric superconductors, Phys. Rev. B **105**, 094518 (2022).

[41] H. D. Scammell, J. Ingham, M. Geier, and T. Li, Intrinsic first- and higher-order topological superconductivity in a doped topological insulator, Phys. Rev. B **105**, 195149 (2022).

[42] C. Le, Z. Yang, F. Cui, A. P. Schnyder, and C.-K. Chiu, Generalized fermion doubling theorems: Classification of two-dimensional nodal systems in terms of wallpaper groups, Phys. Rev. B **106**, 045126 (2022).

[43] C. Timm and A. Bhattacharya, Symmetry, nodal structure, and bogoliubov fermi surfaces for nonlocal pairing, Phys. Rev. B **104**, 094529 (2021).

[44] C. F. B. Lo, H. C. Po, and A. H. Nevidomskyy, Inherited topological superconductivity in two-dimensional dirac semimetals, Phys. Rev. B **105**, 104501 (2022).

[45] J. Yu, Y.-A. Chen, and S. Das Sarma, Euler-obstructed cooper pairing: Nodal superconductivity and hinge Majorana zero modes, Phys. Rev. B **105**, 104515 (2022).

[46] K. Shiozaki, The classification of surface states of topological insulators and superconductors with magnetic point group symmetry, Prog. Theor. Exp. Phys. **2022**, 04A104 (2022).

[47] Z. Zhang, J. Ren, Y. Qi, and C. Fang, Topological classification of intrinsic three-dimensional superconductors using anomalous surface construction, Phys. Rev. B **106**, L121108 (2022).

[48] M. Sato and S. Fujimoto, Topological phases of noncentrosymmetric superconductors: Edge states, Majorana fermions, and non-Abelian statistics, Phys. Rev. B **79**, 094504 (2009).

[49] S. Qin, C. Fang, F.-C. Zhang, and J. Hu, Topological superconductivity in an extended *s*-wave superconductor and its implication to iron-based superconductors, Phys. Rev. X **12**, 011030 (2022).

[50] X.-L. Qi, T. L. Hughes, and S.-C. Zhang, Topological invariants for the Fermi surface of a time-reversal-invariant superconductor, Phys. Rev. B **81**, 134508 (2010).

[51] M. Sato, Y. Tanaka, K. Yada, and T. Yokoyama, Topology of Andreev bound states with flat dispersion, Phys. Rev. B **83**, 224511 (2011).

[52] M. Karoubi, *K-Theory: An Introduction* (Springer Berlin, Heidelberg, 2008).

[53] D. S. Freed and G. W. Moore, Twisted equivariant matter, Ann. Henri Poincaré **14**, 1927 (2013).

[54] K. Shiozaki, M. Sato, and K. Gomi, Atiyah-Hirzebruch spectral sequence in band topology: General formalism and topological invariants for 230 space groups, Phys. Rev. B **106**, 165103 (2022).

[55] H. Song, S.-J. Huang, L. Fu, and M. Hermele, Topological phases protected by point group symmetry, Phys. Rev. X **7**, 011020 (2017).

[56] S.-J. Huang, H. Song, Y.-P. Huang, and M. Hermele, Building crystalline topological phases from lower-dimensional states, Phys. Rev. B **96**, 205106 (2017).

[57] C. Z. Xiong, Minimalist approach to the classification of symmetry protected topological phases, J. Phys. A: Math. Theor. **51**, 445001 (2018).

[58] Z. Song, C. Fang, and Y. Qi, Real-space recipes for general topological crystalline states, Nat. Commun. **11**, 4197 (2020).

[59] K. Shiozaki, C. Z. Xiong, and K. Gomi, Generalized homology and Atiyah–Hirzebruch spectral sequence in crystalline symmetry protected topological phenomena, Prog. Theor. Exp. Phys. **2023**, 083I01 (2023).

[60] Z. Song, S.-J. Huang, Y. Qi, C. Fang, and M. Hermele, Topological states from topological crystals, Sci. Adv. **5**, eaax2007 (2019).

[61] D. V. Else and R. Thorngren, Crystalline topological phases as defect networks, Phys. Rev. B **99**, 115116 (2019).

[62] J.-H. Zhang, Q.-R. Wang, S. Yang, Y. Qi, and Z.-C. Gu, Construction and classification of point-group symmetry-protected topological phases in two-dimensional interacting fermionic systems, Phys. Rev. B **101**, 100501(R) (2020).

[63] A. Rasmussen and Y.-M. Lu, Classification and construction of higher-order symmetry-protected topological phases of interacting bosons, Phys. Rev. B **101**, 085137 (2020).

[64] H. Song, C. Z. Xiong, and S.-J. Huang, Bosonic crystalline symmetry protected topological phases beyond the group cohomology proposal, Phys. Rev. B **101**, 165129 (2020).

[65] B. Peng, Y. Jiang, Z. Fang, H. Weng, and C. Fang, Topological classification and diagnosis in magnetically ordered electronic materials, Phys. Rev. B **105**, 235138 (2022).

[66] More precisely, when $e^{i\theta_g} \neq 1$, the superconducting phase is no longer symmetric under the exact same symmetry g. Nevertheless, the superconducting phase possesses a combined symmetry g with U(1) gauge transformation $c^\dagger_{\boldsymbol{k},\sigma} \to e^{-i\theta_g/2} c^\dagger_{\boldsymbol{k},\sigma}$.

[67] *International Tables for Crystallography*, 5th ed., edited by T. Hahn, Vol. A: Space-group symmetry (Springer, Berlin, 2006).

[68] N. Okuma, M. Sato, and K. Shiozaki, Topological classification under nonmagnetic and magnetic point group symmetry: Application of real-space atiyah-hirzebruch spectral sequence to higher-order topology, Phys. Rev. B **99**, 085127 (2019).

[69] N. Read and D. Green, Paired states of fermions in two dimensions with breaking of parity and time-reversal symmetries and the fractional quantum Hall effect, Phys. Rev. B **61**, 10267 (2000).

[70] M. Stone and S.-B. Chung, Fusion rules and vortices in $p_x + ip_y$ superconductors, Phys. Rev. B **73**, 014505 (2006).

[71] S. Tewari, S. Das Sarma, C. Nayak, C. Zhang, and P. Zoller, Quantum computation using vortices and Majorana zero modes of a $p_x + ip_y$ superfluid of fermionic cold atoms, Phys. Rev. Lett. **98**, 010506 (2007).

[72] S. Tewari, S. Das Sarma, and D.-H. Lee, Index theorem for the zero modes of Majorana fermion vortices in chiral p-Wave superconductors, Phys. Rev. Lett. **99**, 037001 (2007).

[73] V. Gurarie and L. Radzihovsky, Zero modes of two-dimensional chiral p-wave superconductors, Phys. Rev. B **75**, 212509 (2007).

[74] See Supplemental Material at http://link.aps.org/supplemental/10.1103/PhysRevB.109.214502 for the detailed information about AHSS, classification tables, and figures of representative elements of the classifications, which includes Ref. [76].

[75] B. Peng, H. Weng, and C. Fang, Wire construction of class DIII topological crystalline superconductors in two dimensions, Phys. Rev. B **106**, 174512 (2022).

[76] K. Shiozaki and S. Ono, Atiyah-Hirzebruch spectral sequence for topological insulators and superconductors: E_2 pages for 1651 magnetic space groups, arXiv:2304.01827 [cond-mat.mes-hall].